# Structure- and Potential-Dependent Cation Effects on CO Reduction at Copper Single-Crystal Electrodes

Elena Pérez-Gallent, Giulia Marcandalli, Marta Costa Figueiredo, Federico Calle-Vallejo,*,† and Marc T. M. Koper*

Leiden Institute of Chemistry, Leiden University, PO Box 9502, 2300 RA Leiden, The Netherlands

S *Supporting Information*

ABSTRACT: The complexity of the electrocatalytic reduction of CO to CH_4 and C_2H_4 on copper electrodes prevents a straightforward elucidation of the reaction mechanism and the design of new and better catalysts. Although structural and electrolyte effects have been separately studied, there are no reports on structure-sensitive cation effects on the catalyst's selectivity over a wide potential range. Therefore, we investigated CO reduction on Cu(100), Cu(111), and Cu-(polycrystalline) electrodes in 0.1 M alkaline hydroxide electrolytes (LiOH, NaOH, KOH, RbOH, CsOH) between 0 and −1.5 V vs RHE. We used online electrochemical mass spectrometry and high-performance liquid chromatography to determine the product distribution as a function of electrode structure, cation size, and applied potential. First, cation effects are potential dependent, as larger cations increase the selectivity of all electrodes toward ethylene at $E > −0.45$ V vs RHE, but methane is favored at more negative potentials. Second, cation effects are structure-sensitive, as the onset potential for C_2H_4 formation depends on the electrode structure and cation size, whereas that for CH_4 does not. Fourier Transform infrared spectroscopy (FTIR) and density functional theory help to understand how cations favor ethylene over methane at low overpotentials on Cu(100). The rate-determining step to methane and ethylene formation is CO hydrogenation, which is considerably easier in the presence of alkaline cations for a CO dimer compared to a CO monomer. For Li^+ and Na^+, the stabilization is such that hydrogenated dimers are observable with FTIR at low overpotentials. Thus, potential-dependent, structure-sensitive cation effects help steer the selectivity toward specific products.
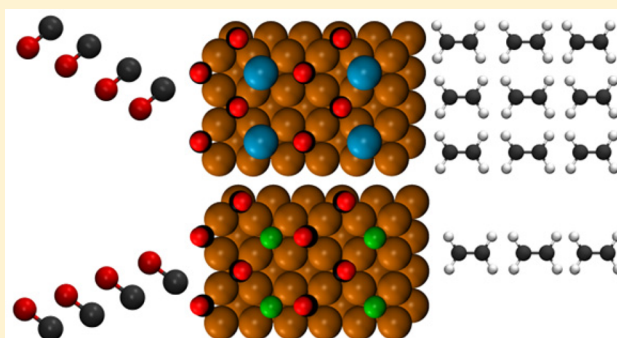
1. INTRODUCTION

Electrocatalytic reduction of CO_2 is an attractive strategy for the conversion of renewable energy into fuels, which helps in closing the biogeochemical carbon cycle. Several metals and other types of electrodes have been studied for the electrochemical reduction of CO_2.[1] However, copper remains the only metal to produce hydrocarbons (primarily methane and ethylene) with reasonable faradaic efficiencies.[2,3] For instance, Jaramillo et al. reported the formation of 16 different species from CO_2 reduction in aqueous bicarbonate solution, where complex molecules including C_2 (e.g., acetaldehyde, acetate, ethylene glycol, glycolaldehyde) and C_3 species (e.g., *n*-propanol, propionaldehyde, allyl alcohol, acetone) were detected with current efficiencies lower than 5%.[4] Several studies of Cu-based catalysts[5,6] have shown higher selectivity for C_2 products. However, the mechanistic reasons for their selectivity remain elusive. Here we examine the combined role of electrolyte cations, potential window, and catalyst structure on the selectivity toward C_1 vs C_2 products during CO reduction on Cu.

Hori et al. showed that CO_2 reduction on Cu electrodes is structure sensitive:[7] Cu(100) electrodes are most efficient for the conversion of CO_2 to C_2H_4, Cu(111) favors the formation of CH_4 and HCOOH, and Cu(110) gives the highest current efficiencies for secondary C_2 products (e.g., acetic acid, acetaldehyde, and ethanol). Similar results were obtained by Schouten et al. during the reduction of CO.[8] While Hori et al. concluded that the introduction of steps on (100) terraces enhances C_2H_4 evolution and suppresses CH_4 formation,[7] Schouten et al. attributed the selective formation of C_2H_4 to pristine (100) terraces.[8] Moreover, they showed that CO reduction to C_2H_4 takes place preferentially at Cu(100) electrodes without simultaneous CH_4 evolution, which indicates that the reaction paths toward CH_4 and C_2H_4 bifurcate in the early stages of CO reduction.[9] On the other hand, it has been shown that C_2 species such as ethylene and ethanol are formed in a common pathway that bifurcates at the late stages of the reaction.[10−12] The favorable formation of C_2H_4 on Cu(100) is supported by density functional theory (DFT) calculations, which demonstrate that C−C bond formation proceeds via CO dimerization and has a lower activation barrier on Cu(100) than on Cu(111).[13,14] In addition to structural effects, there is an important role of the
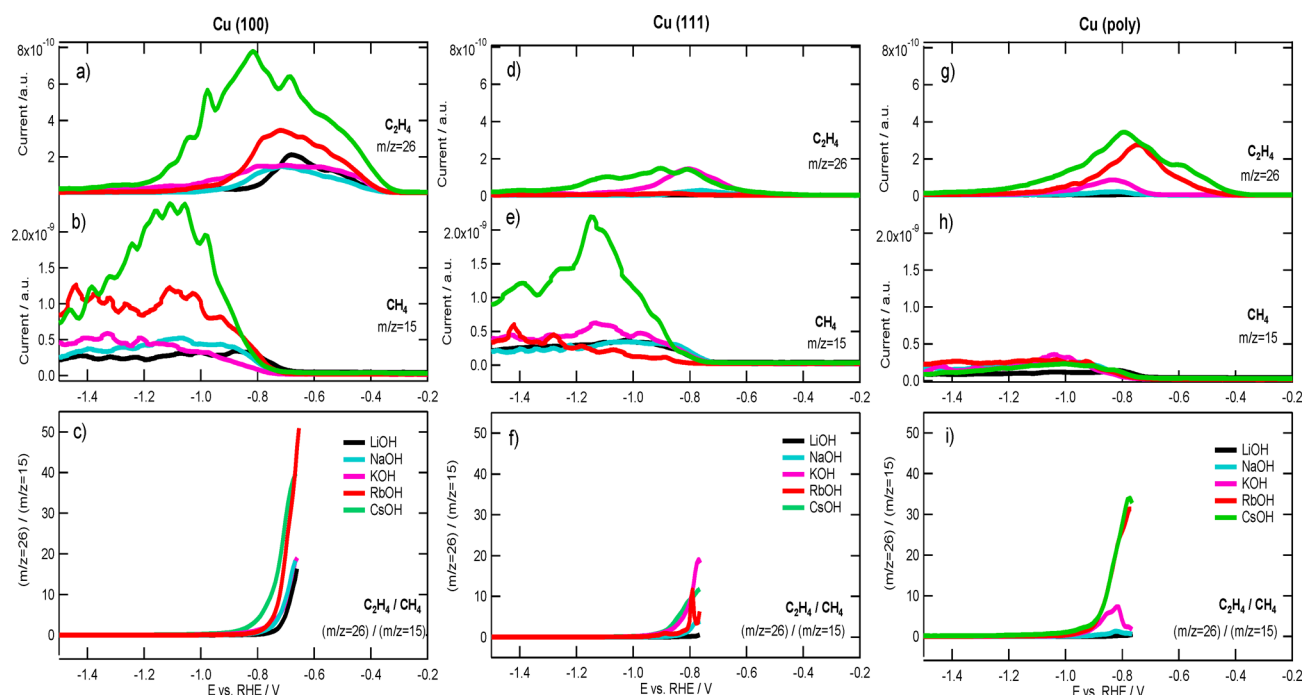
Figure 1. OLEMS mass fragments measured during CO reduction associated with the formation of C_2H_4 (top panel, a, d, and g) and CH_4 (middle panel, b, e, and h) on (a) Cu(100), (b) Cu(111), and (c) polycrystalline Cu for different 0.1 M alkaline hydroxide solutions. Bottom panel (c, f, and i) shows the potential-dependent ratio $(m/z = 26)/(m/z = 15)$ of OLEMS mass fragments associated with the formation of C_2H_4 and CH_4 during CO reduction.

electrolyte, especially through the pH. The onset potential on the NHE scale of CH_4 evolution depends on pH, while C_2H_4 evolution does not. Hori et al. concluded that CO reduction to CH_4 proceeds as a series of concerted proton−electron transfers, in contrast with C_2H_4 evolution, for which the rate-limiting step involves only an early electron transfer, justifying its pH-independent onset.[15,16] We showed previously with DFT calculations that the electron transfer to form a negatively charged $(CO)_2$ dimer is the potential-limiting step of CO reduction to C_2H_4 on Cu(100),[11] in contrast with studies that assume only concerted proton−electron transfers,[17] which cannot explain the pH independence of C_2H_4 formation.

In addition to pH, the activity and selectivity of Cu for CO_2 reduction also depends on the nature of the anions and/or cations in the electrolyte. Strasser et al. showed that the selectivity of the major products of CO_2 reduction depends on the size and concentration of halides:[18] while Cl^- and Br^- enhance the production of CO, I^- lowers CO evolution and increases the selectivity toward methane. The effects were attributed to halide adsorption on copper, which alters the negative charge on the surface and favors the protonation of CO toward CH_4. Furthermore, Lee et al. showed that the presence of Cl^- enhances the catalytic activity toward multiple C_2−C_4 species on Cu-oxide-derived catalysts, due to the presumed advantageous affinity between reaction intermediates and catalytic surface in the presence of Cl^-.[19] Hori et al. reported that alkaline cations affect the selectivity of CO_2 and CO reduction on polycrystalline copper,[10] so that larger cations favor the formation of C_2 and C_3 species such as C_2H_4, C_2H_5OH, and C_3H_7OH. Cation effects were explained by Hori et al. in terms of a variation in the potential in the outer Helmholtz plane (OHP), which originates from a difference in the hydration number of the different cations. Larger cations are less hydrated and expected to adsorb more easily on the

cathode surface, shifting the potential to more positive values, thereby steering the selectivity toward C_2H_4 instead of CH_4. Such experimental observations were confirmed by Kyriacou et al.[20] Bell and co-workers explained cation effects on CO_2 reduction in terms of the different pK_a values for cation hydrolysis, which lower the local pH at the surface from Li^+ to Cs^+ and lead to an increase in CO_2 concentration near the electrode surface.[21] However, this model cannot explain the fact that similar cation effects are observed during CO reduction,[10] the concentration of which is not affected by pH.

All previous studies concerning cation effects in the reduction of CO_2 and CO on copper have used only polycrystalline electrodes and did not cast light on their potential dependence. In the following, we will argue that such effects depend on the electrode structure, the applied potential, and the size of the cation. To this end, we used two single-crystalline copper surfaces (Cu(100), Cu(111)) together with polycrystalline Cu in LiOH, NaOH, KOH, RbOH, and CsOH solutions. Online electrochemical mass spectrometry (OLEMS) and high-performance liquid chromatography (HPLC) were used to investigate the product distribution over a wide potential range. In addition, in situ Fourier transform infrared (FTIR) spectroscopy and DFT calculations are used to identify early reaction intermediates of CO reduction on Cu(100) and explain the cation-mediated enhancement of ethylene formation over methane. Understanding how the structure- and potential-dependent cation effects impact the catalytic performance provides insight for devising efficient and selective catalysts for CO reduction.

2. RESULTS AND DISCUSSION

2.1. OLEMS and HPLC. Cu(111), Cu(100), and Cu(poly) were characterized by voltammetry before and after experiments to control the morphology of the surface;[22] see Figure

S8. The activity and selectivity of the three electrodes toward CO reduction were investigated with OLEMS by varying the alkaline cation in the 0.1 M hydroxide supporting electrolyte. A linear sweep voltammetry between 0 and -1.5 V vs RHE at a scan rate of 1 mV s^{-1} was carried out while simultaneously the volatile products were detected with OLEMS. Figure 1 displays the volatile products formed during the reduction of CO on Cu(100), Cu(111), and polycrystalline Cu for different alkaline hydroxide solutions of identical concentration (0.1 M). Figure 1a−c show the results of CO reduction for Cu(100). The middle panel (b) shows the mass fragment $m/z = 15$ associated with CH$_4$, and the top panel (a) shows the mass fragment $m/z = 26$ associated with C$_2$H$_4$. It is important to note that the reported amounts of products formed are in fact lower than the amounts expected if a purification process of the electrolyte would have been performed, according to the results obtained by Surendranath.[23] The onset potential for CH$_4$ at ca. -0.65 V is independent of the cation in solution. For all cations, except Cs$^+$, the formation of methane reaches a plateau around -0.9 V vs RHE. The general trend is that larger cations increase methane production. Figure 1b also shows that the formation of C$_2$H$_4$ on Cu(100) starts at ca. -0.3 V regardless of the cation. The amount of ethylene formed, as well as its formation rate, increases with the size of the cation. Especially Cs$^+$ shows a significant increase in ethylene production.

On Cu(111) (Figure 1d−f), the onset potential for CH$_4$ is ca. -0.65 V regardless of the cation, with trends in activity similar to Cu(100). (Rb$^+$ deviates from this trend, but, as mentioned in Section S7 in the SI, RbOH frequently showed problems with purity and reproducibility.) The formation of C$_2$H$_4$ starts around -0.4 V regardless of the cation, which is 0.1 V more negative than on Cu(100). The amount of ethylene formed, as well as its formation rate, is highest with Cs$^+$ in the electrolyte. It is important to point out the differences observed with the previous work by Schouten et al.,[9] where the formation of ethylene and methane on Cu(111) displayed a similar profile both having an onset potential of approximately -0.8 V. Similar results were obtained by Nilsson et al.,[5] who found onset potentials for methane and ethylene on Cu(111) close to -0.9 V. However, in this work ethylene formation on Cu(111) starts at lower overpotentials (-0.4 to -0.5 V), which we attribute to the higher sensitivity achieved by using a larger OLEMS tip in combination with the nonmeniscus configuration. Although it is not possible to rule out the contribution of other facets present on the electrode, the significantly higher activity and lower onset potential of Cu(100) surface for ethylene formation is also clearly observed in this work.

On polycrystalline Cu (Figure 1g−i) the onset potential for CH$_4$ production is around -0.65 V regardless of the cation in solution. The plateau is less pronounced than on the single crystals, and the trend with the size of the cation is less evident. C$_2$H$_4$ formation is strongly dependent on the cation, with the smallest cation (Li$^+$) showing essentially no ethylene formation and the largest cation Cs$^+$ showing the strongest selectivity toward ethylene. Although we remark again that it is currently impossible to perform fully quantitative selectivity measurements using OLEMS, the results in Figure 1 allow us to conclude that (i) larger cations enhance CO reduction to ethylene at low overpotentials and the effect is significantly stronger on Cu(100) and (ii) larger cations enhance methane production at high overpotentials.

To support these conclusions, we consider in Figure 1 bottom panels (c, f, and i) the potential dependence of the ratio of the mass signals corresponding to ethylene ($m/z = 26$) and methane ($m/z = 15$) for the three different Cu electrodes. The ratio was plotted as $I(m/z = 26)/I(m/z = 15)$, so a high value expresses a larger production of ethylene over methane. Since at potentials more positive than -0.65 V there is no methane production and the value of the ratio C$_2$/C$_1$ is infinite, the ratio was only calculated in the potential region where both products coexist or the amount of C$_2$H$_4$ detected is null. At low overpotentials, all copper surfaces show a higher selectivity toward ethylene with increasing cation radius, with the highest selectivity achieved for Cu(100), especially with Rb$^+$ and Cs$^+$ in solution. In particular, for a fixed potential of -0.75 V, the ethylene/methane ratio for Cu(100) is 1.59 for Li$^+$, 3.93 for Na$^+$, 4.32 for K$^+$, 7.54 for Rb$^+$, and 14.8 for Cs$^+$ (see Figure S2a). These values show a clear cation effect toward ethylene formation that monotonically follows the cation sizes. In addition, the selectivity for ethylene is enhanced in a larger potential range when larger cations are in solution. Figure S2b shows that larger cations maintain the same selectivity for ethylene at more negative potentials compared to smaller cations: the potentials for which a fixed value of 5 for the ethylene/methane ratio are -0.70, -0.72, -0.72, -0.74, and -0.79 V for Li$^+$, Na$^+$, K$^+$, Rb$^+$, and Cs$^+$. Similar tendencies are observed for Cu(111) and polycrystalline Cu but with significantly lower ratios. The ratio C$_2$/C$_1$ on Cu(111) and polycrystalline Cu in LiOH solution is almost zero over the whole potential range in which both species coexist, indicating low selectivity for ethylene formation over methane in this electrolyte.

Figure S1 shows the mass fragment $m/z = 2$ associated with the formation of H$_2$ from the competitive hydrogen evolution reaction (HER). For all copper surfaces, hydrogen evolution starts at ca. -0.4 V for all different cations except Cs$^+$, for which it starts at slightly less negative potentials. The amount of hydrogen produced as well as its formation rate increases with the size of the cation in the electrolyte for all copper electrodes.

The minor liquid products obtained during CO reduction on polycrystalline copper and their dependence on the nature of the cation were collected and analyzed with HPLC. Due to the low amount of products formed, chronoamperometry experiments for 2 h were carried out using a large copper disk (16.85 mm diameter). Given the long duration of this set of experiments, we did not perform these experiments with single-crystal electrodes, since the stability of the surface structure may be compromised. Chronoamperometry experiments were carried out at three different potentials, -0.5, -0.7, and -0.9 V vs RHE, with different alkaline hydroxides. The concentrations of the obtained products and their cation dependence are summarized in Figure S3. The only liquid product detected for CO reduction at -0.5 V was formic acid. At more negative potentials (-0.7 and -0.9 V) the products obtained were formic acid as a C$_1$ product; acetic acid, glycolic acid, ethylene glycol, and ethanol as C$_2$ products; and propionaldehyde, 1-propanol, and allyl alcohol as C$_3$ products. Such C$_2$ and C$_3$ products obtained during CO reduction have been reported previously.[4,24] In general, larger cations such as Cs$^+$ promote CO reduction to C$_{2+}$ compounds compared to small cations (Li$^+$ and Na$^+$), in agreement with the results of Hori et al.[10] A detailed description of the concentration of the products depending on the cation in solution can be found in the SI, section S2.

Further analysis by ^{1}H NMR was carried out for the samples obtained after 2 h of chronoamperometry at -0.9 V with Na-,
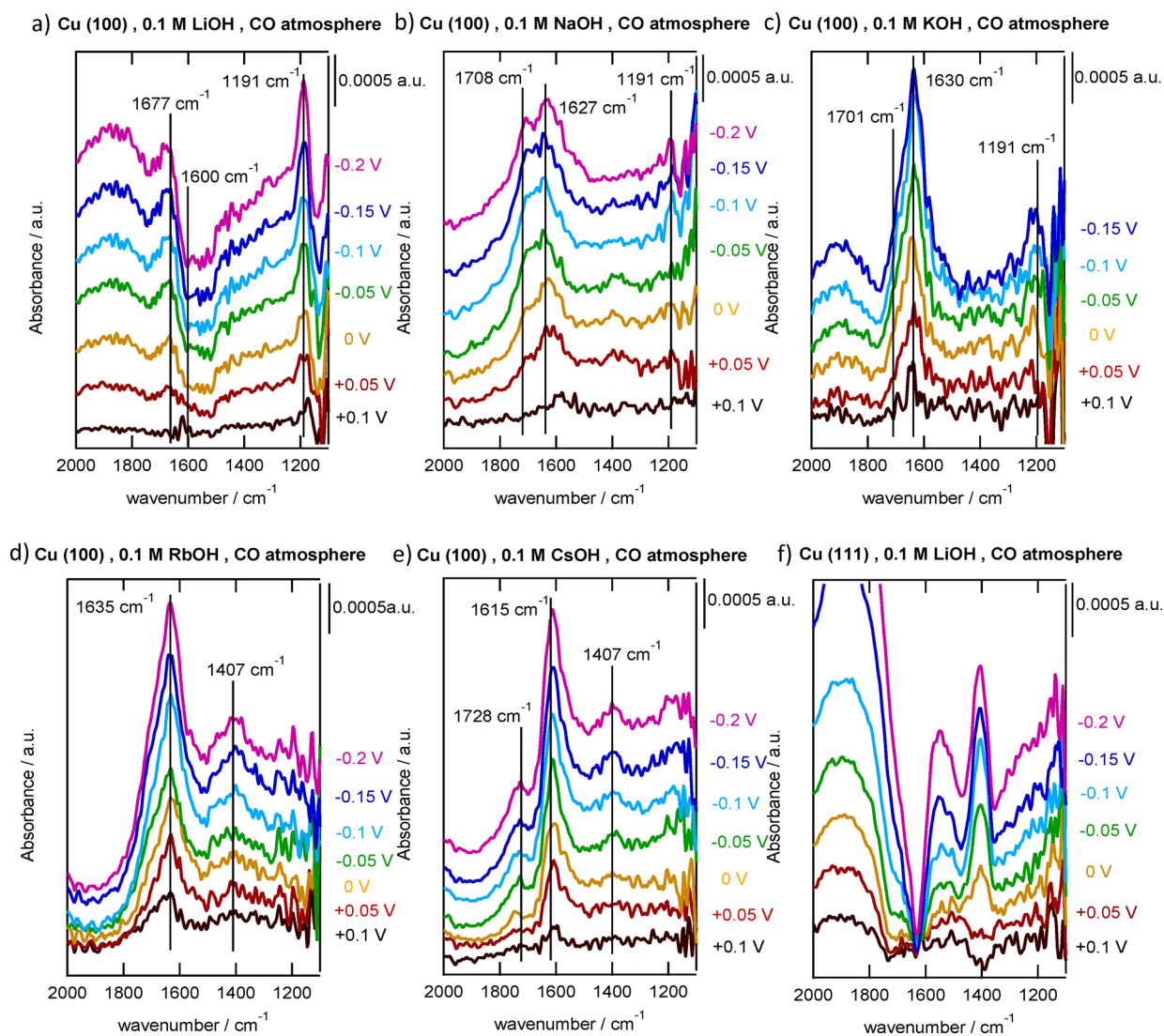
Figure 2. Potential-dependent absorbance spectra of Cu(100) in a CO atmosphere in a 0.1 M solution of (a) LiOH, (b) NaOH, (c) KOH, (d) RbOH, and (e) CsOH. (f) LiOH on Cu(111), provided for comparison. Reference spectrum recorded at +0.1 V vs RHE.

K- and Cs-containing electrolytes (Figure S4 in the SI). The ^{1}H NMR spectra confirmed the products detected with HPLC and their higher concentration with K$^+$ and Cs$^+$ compared to Na$^+$. In addition, methanol was also detected as a reduction product of CO for those three cations. Identification of methanol was not possible with HPLC due to an overlap with the intense peaks of the eluent.

Note that we were unable to consistently detect aldehydes as products, while acetaldehyde and propionaldehyde have been reported to be products of CO$_2$ reduction on copper.[4] This is probably due to the fact that our experiments were carried out at pH 13, and it is known that aldehydes are unstable at such high pH and disproportionate following a Cannizzaro reaction, giving the corresponding carboxylic acid and alcohol.[25]

2.2. FTIR. FTIR spectra were recorded during the early stages of CO reduction on Cu(100) and Cu(111) in different alkaline hydroxide solutions, to gain insight into the dependence of the reaction mechanism on the surface structure of the electrode as well as the cation in the electrolyte. Recent FTIR experiments carried out in Li-containing electrolytes in our group indicated a structure-sensitive process in the early stages of CO reduction,[26] which together with DFT calculations led

us to hypothesize the formation of a hydrogenated CO dimer intermediate in the pathway leading to ethylene, in agreement with previous experimental[8] and theoretical[13] studies. Figure 2a−f show the potential-dependent absorbance spectra of Cu(100) and Cu(111) under a CO atmosphere for different 0.1 M alkaline hydroxide solutions. The spectra recorded on Cu(100) in LiOH solution were previously reported by our group.[26]

The reference spectrum was taken at +0.1 V vs RHE, and additional spectra are provided for +0.05, 0.00, −0.05, −0.10, −0.15, and −0.2 V vs RHE. Due to experimental limitations, it was not possible to record spectra at more negative potentials where the hydrogen evolution reaction starts, as this destabilizes the thin layer formed between the electrode and the prism of the spectrometer, resulting in unstable spectra. These limitations are further explained in section S7 of the Supporting Information. CO reduction in different alkaline hydroxide solutions was also studied on Cu(111) (a representative spectrum is shown in Figure 2f). The FTIR spectra for CO interacting with Cu(100) exhibit two common bands for all alkaline electrolytes. The first band, in the range of 1635−1600 cm^{-1}, corresponds to the O−H bending mode of

H$_2$O. This band causes fluctuations in the baseline of the spectra, making it difficult to identify other bands in this wavenumber range. The second band, in the range of 1730–1670 cm^{-1}, corresponds to the C−O stretching[27−29] of CO adsorbed on hollow sites on Cu(100).[30−33] Apart from these two bands, two other bands arise depending on the electrolyte used. For Li, Na, and K hydroxides, a band at 1191 cm^{-1} attributed to the C−O stretching of a hydrogenated dimer (OCCOH)[26] is observed. Note that the assignment of this band to the hydrogenated dimer and the exclusion of other species were discussed extensively in our previous paper.[26] Besides, in section S8 in the SI we also provide arguments to discard the presence of oxalates. In contrast, the band at 1191 cm^{-1} is not observed when Rb$^+$ and Cs$^+$ are in solution, a feature that will be explained in the next section with DFT calculations. The intensity of the band assigned to C−O stretching of the hydrogenated dimer diminishes from Li to K (Figure 2a−c). For Rb and Cs (Figure 2d,e), a band at 1407 cm^{-1} is observed, which according to the transmission spectra obtained for various species in solution might correspond to formaldehyde. Formaldehyde has been suggested to be an intermediate of the reduction of CO to CH$_4$ on Cu(211).[34,35] The spectra obtained during the reduction of CO on Cu(111) (Figure 2f) also show the band at 1407 cm^{-1}. However, on Cu(111) this band is more intense for smaller cations than for larger cations.

2.3. DFT Calculations. To rationalize some of the observed cation effects, we resort now to DFT calculations. We will focus on Cu(100), as ethylene is formed at low overpotentials and the FTIR results in Figure 2 suggest the presence of a hydrogenated dimer intermediate. Since CO hydrogenation is critical for both methane[17] and ethylene production,[11,36] in the following we will focus only on this step. Figure 3 shows the energetics of the first electrochemical steps in the reduction of one CO molecule to C$_1$ species and two CO molecules to C$_2$ species in a vacuum and in the presence of Li, Na, and Cs (the energies shown are the averages of the separate values found for the three cations; for details see Figures S11 and S12). The first proton−electron transfer for a single CO molecule proceeds as

$$* + CO(g) + H^+ + e^- \rightarrow *CHO \tag{1}$$
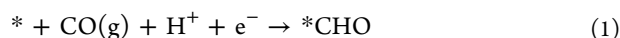
This step consists of CO adsorption and hydrogenation. On the other hand, the first proton−electron transfer for two CO molecules proceeds as

$$* + 2CO(g) + H^+ + e^- \rightarrow *OCCOH \tag{2}$$
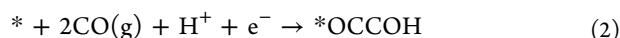
This step comprises successive CO adsorption (denoted *CO and 2*CO in Figure 3), dimerization (*OCCO), and hydrogenation (*OCCOH). The adsorption configurations of C$_1$ and C$_2$ species are provided in Figures S9 and S10.

From Figure 3 it is clear that all intermediates, namely, *CO, 2*CO, *OCCO, *CHO, and *OCCOH, are significantly stabilized by the presence of the alkaline cations, but the strength of the effect depends on the particular adsorbate. Essentially, the overall cation effect is due to the larger stabilization of adsorbates containing C−C bonds (*OCCO and *OCCOH) with respect to the C$_1$ adsorbates (*CO, 2*CO, *CHO). Importantly, the presence of the cations changes the binding mode of the CO dimer, as shown in Figure S9, and the adsorption sites of the adsorbates (Figures S9 and S10).
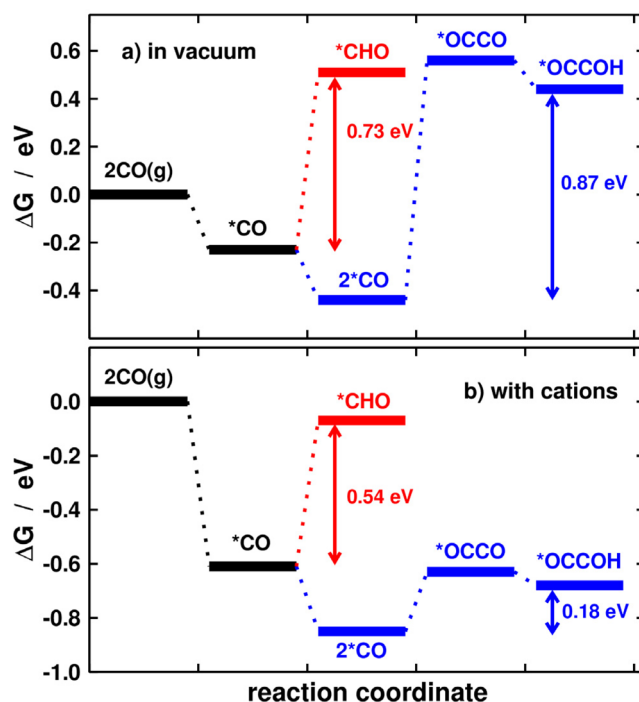

Figure 3. Energetics of the first electrochemical steps of CO reduction for the C$_1$ and C$_2$ pathways on Cu(100) at 0 V vs RHE. (a) In a vacuum and (b) with cations, averaging the energies for Li, Na, and Cs in Figures S11 and S12. While in a vacuum both pathways are highly endothermic, the C$_2$ pathway is remarkably promoted by alkaline cations.

Note that both steps described by eqs 1 and 2 are highly endothermic in the absence of cations, so that the reaction energies for *CO hydrogenation are 0.73 and 0.87 eV for the C$_1$ and C$_2$ pathways (see Tables S2 and S3). In the presence of the cations, the energetics of *CO hydrogenation are lowered from 0.73 eV to 0.54 eV. This change is dwarfed by the dramatic lowering in the C$_2$ pathway from 0.87 eV to 0.18 eV. This attests to a substantial enhancing effect of the alkaline cations by decreasing the energy barriers for *CO reductive coupling. The enhancement of *OCCO with respect to 2*CO clearly illustrates cation effects: the adsorption energy of *OCCO is made more negative by the cations by ∼1.2 eV, whereas the adsorption energy of 2*CO is stabilized by ∼0.4 eV. In sum, Figure 3b explains well the experimentally observed preference of Cu(100) for ethylene formation over methane.

There is also another manifestation of the cation effect, related to the stability of *OCCOH. Similar to the dimer, the hydrogenated counterpart is significantly stabilized (1.16 eV on average) by the presence of alkaline cations. Following the model of Nørskov et al.[17] in which the onset potential is linked to the largest uphill reaction energy in a given pathway, the potential to go from 2*CO to *OCCOH is −0.10 V for Li$^+$, −0.16 for Na$^+$, and −0.28 eV for Cs$^+$ (see Figure S12). Therefore, the hydrogenated dimer should only be observable with FTIR at low potentials (>−0.2 V) in the presence of Li$^+$ and Na$^+$, but not in the case of Cs$^+$, in agreement with the experimental results in Figure 2. This shows that cation effects can be averaged to observe overall trends, but important subtleties pertaining to each cation can only be captured by separate analyses. In addition to the quantitative considerations on the cation effect provided in Figure 3, in section S6 in the SI

we also discuss some qualitative features of Li$^+$, Na$^+$, and Cs$^+$ coadsorption with C$_1$ and C$_2$ species.

2.4. Mechanistic Implications. The OLEMS results in Figure 1 suggest a relation between $m/z = 15$ and $m/z = 26$ (associated with methane and ethylene formation, respectively). Figure 4 illustrates the relation between these two masses for
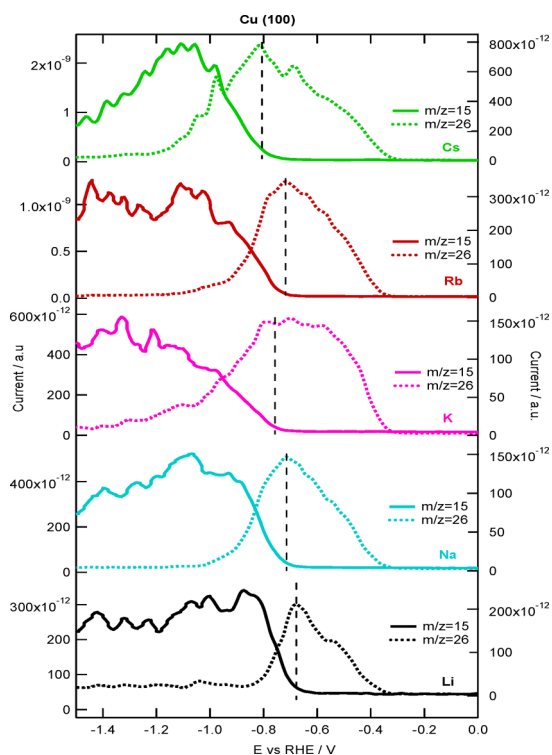

Figure 4. OLEMS mass fragments associated with the reduction products formed during CO reduction on a Cu(100) electrode in different 0.1 M alkaline hydroxide solutions. Dashed lines correspond to $m/z = 26$ associated with the formation of ethylene, plotted against the right axis, and solid lines correspond to $m/z = 15$ associated with the formation of methane, plotted against the left axis. Vertical lines highlight the potential at which the $m/z = 26$ signal associated with ethylene starts to decay.

the specific case of CO reduction on Cu(100), although the trend is also observable for Cu(111) and polycrystalline Cu (see Figure S5 in the SI). Importantly, the mass fragment associated with the formation of ethylene drops when the signal associated with the formation of methane starts to rise. Moreover, the $m/z = 15$ signal increases faster in the electrolytes for which the $m/z = 26$ signal decreases faster, leading to a delay in the potential where the maximum current for methane is observed, depending on the size of the cation. For example, while the decay in ethylene formation in LiOH is acute and the rise of the mass fragment associated with methane is steep, in CsOH solutions the decay of ethylene and the formation of methane are both more gradual. In this order of ideas, larger cations enhance the selectivity toward C$_2$H$_4$ over a wider potential range.

This behavior could be understood if, for instance, methane formation would be the result of C$_2$H$_4$ reduction. However, we discarded this hypothesis because ethylene reduction experiments did not lead to the formation of methane (see Figure S6). It is also important to note that ethane was not detected as a reduction product of ethylene in these experiments.

Therefore, we believe that a cation-, potential-, and facet-dependent picture such as the one in Figure 5 is needed to
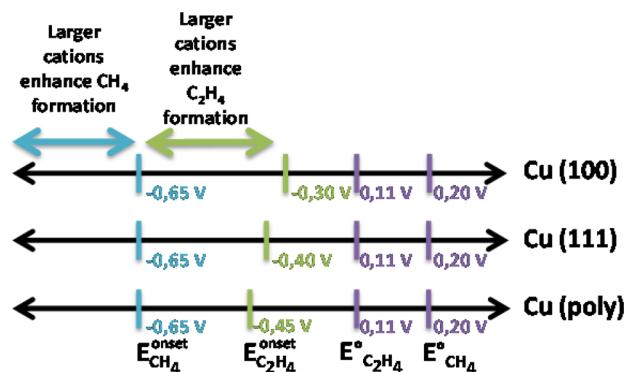
Figure 5. Schematics of the structure- and potential-dependent cation effects for CO reduction toward methane and ethylene in alkaline hydroxide electrolytes (pH = 13). Potentials vs RHE. E^0 are standard equilibrium potentials.

portray the mechanistic effects of alkaline cations on CO reduction. The figure shows a schematic representation of the structure- and potential-dependency of the cation effects for CO reduction toward the two main products, methane and ethylene. The onset potential for ethylene formation depends on the facet, being lower for copper single crystals than for polycrystalline copper. In addition, the onset potential for ethylene is not affected by the cation nature when CO reduction is performed on copper single crystals (see Figure S7), whereas on polycrystalline copper the onset potential varies alongside the cation size, being −0.6 V for Li$^+$ and Na$^+$, −0.4 V for K$^+$, and −0.35 V for Rb$^+$ and Cs$^+$. On the other hand, the onset potential for methane formation is independent of both cation size and surface structure. In the range from −0.3 to −0.65 V, larger cations enhance the formation of ethylene, whereas at potentials more negative than −0.65 V the formation of methane is favored. Figure 4 suggests that this phenomenon is due to a shutting down of the C$_2$ pathway at large overpotentials in which the C$_1$ pathway becomes favorable.

Hori et al. explained the differences in product distribution on the nature of the cation based on the potential distribution at the electrode surface in terms of changes in the outer Helmholtz plane potential.[10] The OHP potential varies with the cations according to their particular adsorption features. Specific adsorption of cations supposedly shifts the OHP potential to more positive values, the OHP potential being higher for Cs$^+$ than for Li$^+$ in view of their dissimilar hydration shells. In this model, a more negative OHP potential translates into a higher H$^+$ concentration, such that the pH at the electrode will decrease as the size of the cation decreases. At higher pH values the formation of ethylene vs methane is enhanced.

On the other hand, in the model proposed by Bell et al.[21] for the cation enhancement of CO$_2$ reduction, the pH near the electrode is lower when larger cations are in solution, leading to a higher local CO$_2$ concentration that results into a higher cathodic activity. They attribute the decrease of pH when larger cations are present to a decrease of the pK_a for the cations' hydrolysis. When the pK_a is sufficiently low, hydrated cations serve as buffering agents, decreasing the pH near the electrode and thereby increasing the local concentration of CO$_2$. Note

that this model is in agreement with experimental data for potentials lower than −1.1 V vs RHE. However, this model cannot explain the fact that similar cation effects are observed during CO reduction,[10] the concentration of which is not affected by (local) pH. In their model, Bell et al. explained that the hydrolysis of hydrated cations is only effective in mildly basic or acidic electrolytes. However, our experimental results showed a cation enhancement for the production of ethylene during CO reduction in strongly alkaline media (pH = 13).

Our explanation of cation effects is based on Figures 3, S11, and S12. We believe that cations are essentially catalytic promoters, their presence altering substantially the free-energy landscape of CO reduction. They especially stabilize C_2 species by means of strong O-cation interactions, justified by the strong tendency of those species (e.g., *OCCO and *OCCOH) to be negatively charged, unlike isolated *CO monomers. Our perspective on cation effects is in line with that of Janik and co-workers,[37] who explicitly included cation, anion, and solvation effects in their calculations and reported similar effects for CO_2 reduction in the presence of K^+. The averaging in Figure 3 is close to that of Nørskov and co-workers,[38,39] who have shown that cations at the double layer induce local field effects that alter the adsorption energies. Although overall cation effects can be averaged, we stress that subtle yet important details such as differences in adsorption sites, adsorption configurations (Figures S9 and S10), and onset potentials as a function of cation size (Figures S11 and S12) are only captured when modeling the cations explicitly.

Finally, it is important to note that the present work is devoted only to "fully metallic" Cu electrodes, while "oxide-derived" Cu electrodes also exist and, due to their high activity for CO reduction, are the subject of extensive research.[5,40−42] "Fully metallic" Cu(100) and oxide-derived Cu electrodes both produce large amounts of C_2 products, although the former is inclined toward ethylene, while the latter favors ethanol. Our previous works provided a plausible explanation for such dissimilar behavior: there is a selectivity-determining intermediate in the CO reduction pathway to C_2 products, namely, *CH_2CHO.[11] If hydrogenation leads to *CH_3CHO (i.e., adsorbed acetaldehyde), ethanol is the major final product.[12] Conversely, if hydrogenation leads to *CH_2CH_2O, then ethylene is favored.[11] Whereas acetaldehyde is reduced to ethanol at larger rates at steps and grain boundaries[12,43] compared to terraces, pristine (100) terraces are known to favor ethylene production.[8,9]

3. CONCLUSIONS

In this paper, we have shown that the combined effect of alkaline cations and catalyst morphology can steer the selectivity of CO reduction toward ethylene or methane, depending on the potential. Specifically, our results suggest the following conclusions.

(1) In general, larger cations enhance CO reduction to ethylene at low overpotentials, especially on Cu(100). With smaller cations in solution, CO reduction on Cu(111) and Cu(polycrystalline) shows low selectivity for ethylene formation over methane over the whole potential range in which both species coexist. The formation of other minor C_2 and C_3 products (such as acetic acid, glycolic acid, ethanol, and propanol) is also enhanced by the presence of larger cations.

(2) A correlation between the decline of ethylene formation and the onset potential for methane formation was observed. Furthermore, methane formation reaches its plateau when ethylene formation drops to zero. This suggests that the C_2 pathway is blocked by the enhancement of the C_1 pathway. This correlation depends on the cation size, so that larger cations enhance the selectivity toward ethylene over a wider potential range.

(3) For the two major products, methane and ethylene, differences in the onset potential were found as a function of the cation size and the surface structure. While the onset potential of ethylene formation depends on these two factors, the onset potential of methane does not.

(4) FTIR and DFT calculations were used to gain insight into the origin of cation effects on Cu(100). As described elsewhere,[26] FTIR suggests the presence of a hydrogenated dimer intermediate (OCCOH) at low overpotentials. The formation of this intermediate depends on the size of the cation, so that the hydrogenated dimer can be detected with FTIR in the presence of Li^+, Na^+, and K^+, but not in the presence of Rb^+ or Cs^+. DFT calculations explain that the potential necessary to form *OCCOH from *CO in the presence of Cs^+ is more negative compared to Li^+ or Na^+. Besides, the adsorption energies of species containing C−C bonds are dramatically stabilized by cations with respect to C_1 species, justifying the selectivity toward ethylene at low overpotentials.

(5) The role of cations in CO reduction is that of a catalytic promoter, changing the free energy landscape of CO reduction and specifically stabilizing certain intermediates, especially those with a favorable (electrostatic) interaction with the cation. Larger cations such as Cs promote pathways with these intermediates more effectively than smaller cations such as Li.

4. METHODS

4.1. Experimental Section. Experimental methods are explained in detail in section S7 of the Supporting Information.

4.2. Computational. The DFT total energies were calculated with VASP,[44] making use of the projector augmented wave (PAW) method[45] and the PBE exchange−correlation functional.[46] Further details are provided in section S6 in the SI.

■ ASSOCIATED CONTENT

ⓢ Supporting Information

The Supporting Information is available free of charge on the ACS Publications website at DOI: 10.1021/jacs.7b10142.

> Hydrogen evolution reaction, HPLC measurements, ^{1}H NMR spectra, additional mechanistic implications, electrode surface characterization, additional computational details, experimental methods, exclusion of the formation of oxalates (PDF)

■ AUTHOR INFORMATION

Corresponding Authors
*f.calle.vallejo@chem.leidenuniv.nl
*m.koper@chem.leidenuniv.nl

ORCID ⓞ
Federico Calle-Vallejo: 0000-0001-5147-8635
Marc T. M. Koper: 0000-0001-6777-4594

Present Address
†Departament de Ciència de Materials i Química Física & Institut de Química Teòrica i Computacional (IQTCUB), Universitat de Barcelona, Martí i Franqués 1, 08028 Barcelona, Spain.

Notes

The authors declare no competing financial interest.

■ REFERENCES

(1) Hori, Y. In *Modern Aspects of Electrochemistry*; Springer: New York, 2008; pp 89−189.

(2) Hori, Y.; Kikuchi, K.; Murata, A.; Suzuki, S. *Chem. Lett.* **1986**, *15*, 897−898.

(3) Hori, Y.; Kikuchi, K.; Suzuki, S. *Chem. Lett.* **1985**, *14*, 1695−1698.

(4) Kuhl, K. P.; Cave, E. R.; Abram, D. N.; Jaramillo, T. F. *Energy Environ. Sci.* **2012**, *5*, 7050−7059.

(5) Roberts, F. S.; Kuhl, K. P.; Nilsson, A. *Angew. Chem., Int. Ed.* **2015**, *54*, 5179−5182.

(6) Li, C. W.; Ciston, J.; Kanan, M. W. *Nature* **2014**, *508*, 504−507.

(7) Hori, Y.; Takahashi, I.; Koga, O.; Hoshi, N. *J. Mol. Catal. A: Chem.* **2003**, *199*, 39−47.

(8) Schouten, K. J. P.; Pérez Gallent, E.; Koper, M. T. *ACS Catal.* **2013**, *3*, 1292−1295.

(9) Schouten, K. J. P.; Qin, Z.; Gallent, E. P.; Koper, M. T. M. *J. Am. Chem. Soc.* **2012**, *134*, 9864−9867.

(10) Murata, A.; Hori, Y. *Bull. Chem. Soc. Jpn.* **1991**, *64*, 123−127.

(11) Calle-Vallejo, F.; Koper, M. *Angew. Chem., Int. Ed.* **2013**, *52*, 7282−7285.

(12) Ledezma-Yanez, I.; Gallent, E. P.; Koper, M. T.; Calle-Vallejo, F. *Catal. Today* **2016**, *262*, 90−94.

(13) Li, H.; Li, Y.; Koper, M. T.; Calle-Vallejo, F. *J. Am. Chem. Soc.* **2014**, *136*, 15694−15701.

(14) Montoya, J. H.; Shi, C.; Chan, K.; Nørskov, J. K. *J. Phys. Chem. Lett.* **2015**, *6*, 2032−2037.

(15) Hori, Y.; Takahashi, R.; Yoshinami, Y.; Murata, A. *J. Phys. Chem. B* **1997**, *101*, 7075−7081.

(16) Gattrell, M.; Gupta, N.; Co, A. *J. Electroanal. Chem.* **2006**, *594*, 1−19.

(17) Peterson, A. A.; Abild-Pedersen, F.; Studt, F.; Rossmeisl, J.; Nørskov, J. K. *Energy Environ. Sci.* **2010**, *3*, 1311−1315.

(18) Varela, A. S.; Ju, W.; Reier, T.; Strasser, P. *ACS Catal.* **2016**, *6*, 2136−2144.

(19) Lee, S.; Kim, D.; Lee, J. *Angew. Chem.* **2015**, *127*, 14914−14918.

(20) Kyriacou, G.; Anagnostopoulos, A. *J. Appl. Electrochem.* **1993**, *23*, 483−486.

(21) Singh, M. R.; Kwon, Y.; Lum, Y.; Ager, J. W., III; Bell, A. T. *J. Am. Chem. Soc.* **2016**, *138*, 13006−13012.

(22) Schouten, K. J. P.; Gallent, E. P.; Koper, M. T. *J. Electroanal. Chem.* **2013**, *699*, 6−9.

(23) Wuttig, A.; Surendranath, Y. *ACS Catal.* **2015**, *5*, 4479−4484.

(24) Hori, Y.; Takahashi, R.; Yoshinami, Y.; Murata, A. *J. Phys. Chem. B* **1997**, *101*, 7075−7081.

(25) Birdja, Y. Y.; Koper, M. T. M. *J. Am. Chem. Soc.* **2017**, *139*, 2030−2034.

(26) Pérez-Gallent, E.; Figueiredo, M. C.; Calle-Vallejo, F.; Koper, M. *Angew. Chem.* **2017**, *129*, 3675−3678.

(27) Hori, Y.; Koga, O.; Watanabe, Y.; Matsuo, T. *Electrochim. Acta* **1998**, *44*, 1389−1395.

(28) Ryberg, R. *Surf. Sci.* **1982**, *114*, 627−641.

(29) Gajdoš, M.; Hafner, J. *Surf. Sci.* **2005**, *590*, 117−126.

(30) Chang, S. C.; Weaver, M. J. *J. Phys. Chem.* **1990**, *94*, 5095−5102.

(31) Arán-Ais, R. M.; Figueiredo, M. C.; Vidal-Iglesias, F. J.; Climent, V.; Herrero, E.; Feliu, J. M. *Electrochim. Acta* **2011**, *58*, 184−192.

(32) Shaw, S. K.; Berná, A.; Feliu, J. M.; Nichols, R. J.; Jacob, T.; Schiffrin, D. *J. Phys. Chem. Chem. Phys.* **2011**, *13*, 5242−5251.

(33) Koper, M. T.; van Santen, R. A. *J. Electroanal. Chem.* **1999**, *476*, 64−70.

(34) Cook, R. L.; MacDuff, R. C.; Sammells, A. F. *J. Electrochem. Soc.* **1989**, *136*, 1982−1984.

(35) DeWulf, D. W.; Jin, T.; Bard, A. J. *J. Electrochem. Soc.* **1989**, *136*, 1686−1691.

(36) Hori, Y.; Murata, A.; Takahashi, R.; Suzuki, S. *J. Am. Chem. Soc.* **1987**, *109*, 5022−5023.

(37) Akhade, S. A.; McCrum, I. T.; Janik, M. J. *J. Electrochem. Soc.* **2016**, *163*, F477−F484.

(38) Sandberg, R. B.; Montoya, J. H.; Chan, K.; Nørskov, J. K. *Surf. Sci.* **2016**, *654*, 56−62.

(39) Chen, L. D.; Urushihara, M.; Chan, K.; Nørskov, J. K. *ACS Catal.* **2016**, *6*, 7133−7139.

(40) Kim, Y.-G.; Javier, A.; Baricuatro, J. H.; Soriaga, M. P. *Electrocatalysis* **2016**, *7*, 391−399.

(41) Verdaguer-Casadevall, A.; Li, C. W.; Johansson, T. P.; Scott, S. B.; McKeown, J. T.; Kumar, M.; Stephens, I. E.; Kanan, M. W.; Chorkendorff, I. *J. Am. Chem. Soc.* **2015**, *137*, 9808−9811.

(42) Gao, D.; Zegkinoglou, I.; Divins, N. J.; Scholten, F.; Sinev, I.; Grosse, P.; Roldan Cuenya, B. *ACS Nano* **2017**, *11*, 4825−4831.

(43) Bertheussen, E.; Verdaguer-Casadevall, A.; Ravasio, D.; Montoya, J. H.; Trimarco, D. B.; Roy, C.; Meier, S.; Wendland, J.; Nørskov, J. K.; Stephens, I. E. *Angew. Chem., Int. Ed.* **2016**, *55*, 1450−1454.

(44) Kresse, G.; Furthmüller, J. *Phys. Rev. B: Condens. Matter Mater. Phys.* **1996**, *54*, 11169−11186.

(45) Kresse, G.; Joubert, D. *Phys. Rev. B: Condens. Matter Mater. Phys.* **1999**, *59*, 1758−1775.

(46) Perdew, J. P.; Burke, K.; Ernzerhof, M. *Phys. Rev. Lett.* **1996**, *77*, 3865−3868.